water

MDPI

Article

Contrasting the Optical Characterization of Dissolved Organic Matter in Water and Sediment from a Nascent River-Type Lake (Chongqing, China)

Fengxia Niu [1,2,*,†], Fangying Ji [1,2,*], Qian Zhang [1,2] and Qiushi Shen [1,2]

[1] Key Laboratory of the Three Gorges Reservoir Region's Eco-Environment, Ministry of Education, Chongqing University, Chongqing 400045, China; zhangqiancqu@cqu.edu.cn (Q.Z.); m15025439561@126.com (Q.S.)
[2] National Centre for International Research of Low-Carbon and Green Buildings, Chongqing University, Chongqing 400045, China
* Correspondence: nfxctguedu@yeah.net (F.N.); jfy@cqu.edu.cn (F.J.)
† Current address: College of Hydraulic & Environmental Engineering, China Three Gorges University, Yichang 443002, China.

Abstract: Carbon cycling in rivers is altered by the creation of impoundments through dam construction. This paper seeks to identify the source and composition of dissolved organic matter (DOM) in both water and sediment in Lake Longjing by contrasting the optical characterization of DOM. By comparing the dissolved organic carbon (DOC) concentrations, we show that the sediment (53.7 ± 16.6 mg/L) acts as a DOC source to the overlying water (23.1 ± 1.4 mg/L). The estimated DOC flux in the original reservoir region (88.3 mg m^{-2} d^{-1}) is higher than that in the newly submerged region (26 mg m^{-2} d^{-1}), whereas the latter has larger contribution to the DOC annual load because of its larger sediment area. Spectroscopic analysis suggested that pore waters had higher aromaticity and lower proportion of fresh DOM than those in surface waters and benthic overlying waters. Through Parallel Factor Analysis, four fluorescent components were identified, i.e., two terrestrial humic-like components, one protein-like, and one microbial humic-like. Spearman correlation and Non-Metric-Multidimensional Scaling (NMDS) analysis manifested that fluorescent DOM in surface sediments is mainly contributed by autochthonous source, the others by allochthonous source. Due to the high sensitivity of the fluorescent intensity of the protein-like component, it is a useful indicator to reveal the changes of source of DOM.

Keywords: sediments; dissolved organic matter; EEM-PARAFAC

Citation: Niu, F.; Ji, F.; Zhang, Q.; Shen, Q. Contrasting the Optical Characterization of Dissolved Organic Matter in Water and Sediment from a Nascent River-Type Lake (Chongqing, China). *Water* **2021**, *13*, 70. https://doi.org/10.3390/w13010070

Received: 11 October 2020
Accepted: 27 December 2020
Published: 31 December 2020

1. Introduction

Worldwide construction in dams has occurred at a rapid pace over the past several decades such that approximately 50% of river water is directly or indirectly controlled by reservoirs before reaching an ocean [1,2]. Dam reservoirs inevitably break the connectivity of rivers and become an increasingly important component of inland waters [3]. Compared with natural fluvial ecosystem, the aquatic habitat of reservoirs has changed, characterized by longer water retention time, slower flow rate and stronger sediment retention ability. This leads to alterations of the source and composition of organic matters in water bodies [4]. As a central constituent of carbon cycle, dissolved organic matter (DOM) in sediments plays a key role in the transport and transformation of xenobiotics [5–7]. Changes in DOM quality and origin affect sediment microbial communities along the river continuum [8]. In some aquatic ecosystems, DOM in sediment pore waters has been found at higher level than those in corresponding overlying waters [1,9], indicating a net upward flux of DOM exists across the sediment-water interface, which eventually results in negative consequences for ecosystem function and water quality [10]. A recent report [1] focuses on the dynamics of DOM in river sediments after impoundment and found that total organic

carbon (TOC) concentrations in surface waters increased with time, and the sediment acts as one of the TOC sources. Based on laboratory benthic chamber experiment and overall estimation, the global inland benthic efflux of DOC reached up to 0.10 Gt a^{-1} [5].

Currently diverse analytical techniques have been applied to explore DOM structures, compositions, and molecular sizes [5,6,11]. Among these techniques, the ultraviolet-visible (UV-Vis) absorption and fluorescence spectroscopic analysis has high sensitivity and it does not require extraction and pre-concentration procedures prior to measurements [5]. This technique was applied for investigating the structure and composition of DOM in sediment pore water sampled from marine [12], estuaries [13–15], rivers [16,17], and lakes [18,19]. Interestingly, parallel factor analysis (PARAFAC) was applied to survey the DOM sources of pore waters in four Chinese lakes [19]. The results revealed that DOM mainly comprised two fulvic acid-like components with mixed sources of both allochthonous and autochthonous. Nevertheless, their investigation could be furthered by comparing the fluorescent components of DOM between pore water and overlying water, and measuring other optical indicators besides specific UV absorbance at 254 nm ($SUVA_{254}$). However, few investigations have delved into the source identification and change trend of sediment DOM from artificial lakes or reservoirs [20]. Therefore, it is necessary to identify and compare the sources and compositions of DOM in water and sediment from the artificial environments.

In this study, the optical characterization of DOM derived from surface water (SW), benthic overlying water (OW), and pore water (PW) in a nascent artificial lake (Lake Longjing (LLJ)) was compared by spectral indicators and PARAFAC analysis. Since LLJ was constructed by dam heightening and no desilting was carried out before impoundment, the sediment region in this lake comprises both original reservoir and newly submerged regions. The objectives are to (1) discuss the source or sink characteristics of DOC in the sediments of LLJ; (2) reveal the differences of DOM properties in PWs with SWs and with OWs, respectively; (3) identify the source and composition of DOM in water and sediment from this lake.

2. Materials and Methods

2.1. Site Description

LLJ as a nascent river-type lake located in the center of Chongqing Garden Expro Park (Figure 1), Western China, was newly formed by heightening the downstream dam in 2012 [21]. Its water area is 0.67 km^2, with the catchment area of 11.8 km^2 and the reservoir capacity of 6.63 million m^3 [22]. The Zhaojiaxi and Longjinggou Rivers were formerly tributaries to LLJ, but rainfall runoff is now the main water supply due to extensive hydrologic modifications of the lake and its watershed in 2014 [23]. The abundant annual rainfall usually occurs between May and September, which is typical of a humid subtropical monsoon climate. Since LLJ is surrounded by many hills [24], it has the topographic and geomorphic features of mountainous lake, resulting in the formation of many lake bays with slow water velocity. These lake bays have relatively shallow water depth (~10 m), while the open water area in front of the dam has the maximum water depth of 22 m [23]. During the initial impoundment period, water quality indicated that LLJ was mesotrophic. The hydrological characteristics of this lake were of relatively high water level, slow water flow velocity, long water residence time (2.5 year), low level of dissolved oxygen (DO) in bottom water, and etc. [21].

In addition, LLJ sediments are composed of different sedimentary types. The sediment organic matter distributes heterogeneously since the sediment in original reservoir region was not dredged before impoundment. According to the difference in sedimentary histories, we conceptually divide the lake into three regions, i.e., original reservoir subregion, newly submerged bottom and slope subregions [24]. The sediments in original reservoir subregion had thick, dark and smelly peat layers [21]. The newly submerged slope subregion was close to lake shores and had relatively low water depth, the terrain of which was steep and not prone to the accumulation of particles and organic debris. In

contrast, the newly submerged bottom subregion is located between the original reservoir and newly submerged slope subregions. It was formerly mountain forest or farmland; a portion of its original vegetation and soil were retained after water storage.

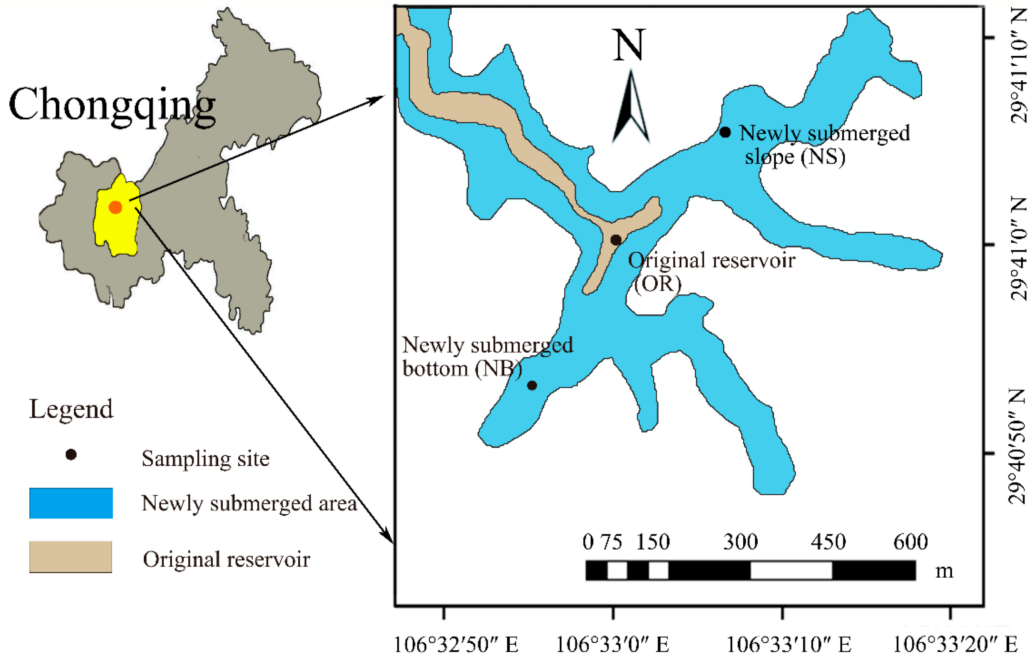

Figure 1. Locations of three sampling sites in LLJ.

2.2. Sampling and Preprocessing

Three representative sampling sites were shown in Figure 1. They were selected to be representative of the original reservoir (OR; 29°41′00″ N, 106°33′00″ E), newly submerged bottom (NB; 29°40′53″ N, 106°32′55″ E) and slope (NS; 29°41′05″ N, 106°33′08″ E) subregions. OR was located at the center of the lake, with deep water depth. Both NB and NS were located in the lake bays, and NB was located near the Northern Garden Bay. Intact sediment cores were collected on 26 October 2015 with a gravity corer (Uwitec—Niederreiter Richard, Mondsee, Austria) from the three sampling sites (OR, NB and NS). These cores each comprised approximately 40 cm depth of overlying water column and 15 cm depth of sediment core. At the same time, the corresponding surface-water (SW, 0.5 m below the lake water surface) samples at each site were collected into acid-washed glass bottles.

Water temperature and other physicochemical parameters were measured in situ using calibrated electrodes (HACH, HQ 40d, Loveland, CO, USA). Overlying-water (OW, 5 cm) samples close to the sediment-water interface were injected into glass bottles at an interval of 1 cm and then the corresponding subsamples of sediments (10 cm at OR and NB, and 6 cm at NS) were sliced into sections at 1 cm length sequentially from top layers down to the bottom. Three duplicate sediment cores were collected for each sample, and the three replicates in each layer were mixed homogeneously [25]. Then, the mixed subsamples of sediments were fully packed in polyethylene centrifuge tubes. Note that all these water samples and sediment samples were kept at 4 °C prior to analyses which were completed within 24 h.

2.3. Analytical Measurements of PW and DOC Flux Estimation

Sediment pore-water (PW) samples were the extracted supernatants obtained by centrifugation at 4000 rpm with 10 min. All water samples (SW, OW and PW) were filtered through 0.45 µm polypropylene syringe filters (Whatman GD/X) prior to DOC analysis, UV-Vis absorption, and fluorescence measurements. The DOC concentrations

were determined by high-temperature catalytic oxidation (HTCO) on a LiquiTOII Analyzer (Elementar, Langenselbold, Germany).

To estimate benthic DOC flux, Fick's first law of diffusion was used, shown in Equation (1) [1]. This equation assumes that solute diffusion is the dominant transport mechanism across the sediment-water interface, and advection, resuspension as well as bioturbation are neglected:

$$J = -\phi D_s (\partial c/\partial x)_{x=0}, \quad (1)$$

where J is the benthic flux, ϕ is the porosity of surface sediment (0–1 cm) [26], D_s is the diffusion coefficient, and $(\partial c/\partial x)_{x=0}$ is DOC concentration gradient across the sediment-water interface [27]. Combined benthic flux with lake sediment area, the annual load of DOC (W, t/a) from sediments was estimated through Equation (2) [21]:

$$W = \sum_{i}^{n} J_i \times A_i \times 365 \times 10^{-9}, \quad (2)$$

where A_i represents the sediment area of each subregion according to different sedimentary histories [24].

2.4. Absorbance Measurement

Both absorbance and fluorescence were measured at room temperature (25 ± 2 °C) and Milli-Q water was used as a blank sample. Absorbance spectra were obtained between 200–700 nm at 1 nm interval using a UV-Vis absorbance spectrophotometer (U-3010, Hitachi Ltd., Tokyo, Japan) with a 1 cm quartz cuvette. Baseline correction was conducted by subtracting offset values from the absorbance spectra of blank water.

Three absorption indicators were used including spectral slope ratio (S_R), absorption ratio (E_2/E_3) and specific UV absorbance at 254 nm ($SUVA_{254}$). The formulae of these indicators are listed below in Table 1.

Table 1. Summary of absorption and fluorescence indicators.

Formula	Calculation	Purpose
$S_R = \frac{S_{275-295}}{S_{350-400}}$	Spectral slopes from 275 to 295 and 350 to 400 nm ($S_{275-295}$ and $S_{350-400}$, respectively) were calculated by performing linear regressions of the natural log transformed absorbance spectra [28].	A proxy (inversely related) for DOM molecular weight [28]
$E_2/E_3 = \frac{a_{250}}{a_{365}}$	The ratio of Naperian absorption coefficients at 250 to 365 nm [29,30].	To estimate relative molecular size of DOM [31]
$SUVA_{254} = \frac{a_{254}}{C_{DOC}}$	Calculated by dividing the absorption at wavelength 254 (a_{254}, m^{-1}) by DOC concentration (C_{DOC}, mg/L).	A proxy for aromaticity [32]
$FI = \frac{F_{\lambda_{Ex=370},\ \lambda_{Em=470}}}{F_{\lambda_{Ex=370},\ \lambda_{Em=520}}}$	The ratio of Em 470 nm and Em 520 nm at Ex at 370 nm for instrument-corrected spectra [33].	To distinguish the terrestrially- and microbially-derived DOMs [34]
$BIX = \frac{F_{\lambda_{Ex=310},\ \lambda_{Em=380}}}{F_{\lambda_{Ex=310},\ \lambda_{Em=430}}}$	The ratio of Em 380 nm and Em 430 nm at Ex 310 nm [35].	An indicator of recent autotrophic productivity [35]

Note: BIX: biological index; FI: fluorescence index; Em: emition; Ex: excitation.

2.5. Fluorescence Measurement

Excitation-emission matrix (EEM) fluorescence spectra of water samples were measured using an F-7000 fluorescence spectrometer (Hitachi Ltd., Tokyo, Japan) with a 1 cm quartz cuvette. The emission (Em) wavelength was obtained between 250–600 nm and the excitation (Ex) wavelength was obtained between 200–450 nm at 5 nm intervals. The scan mode was 700-voltage xenon lamp and the scan speed was 1200 nm·min^{-1} with slit widths of 5 nm. The fluorescence spectra were corrected for instrumental biases according to the Hitachi procedure. Fluorescence index (FI) and biological index (BIX) were the ratios of emission wavelengths as listed in Table 1.

Four preprocesses are required to obtain fluorescent components of DOM, and they were all performed using MATLAB R2014a (The MathWorks, Natick, Massachusetts State,

USA). First, water Raman scatter peaks were removed by subtracting the EEMs of Milli-Q water blanks. Second, fluorescence intensities ($F_{\lambda Ex, \lambda Em}$) were provided in Raman units (RU, Equation (3)) to remove instrument-dependent intensity factors [36], where A_{rp} = the integral of the water Raman peak from Ex = 350 nm.

$$F_{\lambda_{Ex,}\,\lambda_{Em}}\,(\mathrm{RU}) = \frac{F^{Corr}_{\lambda_{Ex,}\,\lambda_{Em}}\,(\mathrm{AU})}{\mathrm{A}_{\,\mathrm{rp}}} \quad (3)$$

Third, correction for inner-filter effects on EEM measurements (Equation (4)) was performed by adjusting DOM absorbance at the corresponding wavelengths [37].

$$F^{Corr}_{\lambda_{Ex,}\,\lambda_{Em}} = F^{Obs}_{\lambda_{Ex,}\,\lambda_{Em}} \times 10^{0.5\,\times(A_{\lambda Ex}+A_{\lambda Em})} \quad (4)$$

Last, Rayleigh scatter was eliminated using the DOMFluor toolbox [38]. It is notable that excitation wavelengths below 225 nm and emission wavelengths below 300 nm and above 550 nm were removed in the following analysis so as to avoid deteriorating signal to noise ratios [39,40].

2.6. PARAFAC Modelling

Fluorescent DOM (FDOM) components were further identified using PARAFAC analysis which separates a set of EEMs data into independent components. PARAFAC analysis was conducted with the above-mentioned DOMFluor toolbox. A 4-component model was well validated through a specific method of split half analysis which split the EEMs data into two halves and each half was modelled independently. Then residual analysis was conducted to determine the number of components through comparing the residuals of increased number of components. To quantify and compare the differences of FDOM components in water samples, the abundance and location of each component were estimated based on the maximum fluorescent intensity (F_{max}) and Ex/Em loading in the model.

2.7. Statistical Analysis

Differences in DOC concentrations and DOM optical indicators (i.e., S_R, $SUVA_{254}$, E_2/E_3, FI, and BIX) between OWs and PWs from three sampling sites were determined through one-way analysis of variance (one-way ANOVA). The significance of the statistical test was determined at the 0.05 level. Statistical analysis of Spearman correlation between PARAFAC components (C1–C4) and DOM optical indicators was conducted by SPSS 24 software (IBM SPSS, Inc., Chicago, IL, USA). The non-Metric-Multidimensional Scaling (NMDS) analysis was performed and the Bray–Curtis distance was selected herein to visualize the spatial distribution of water samples based on above DOM parameters. The ordination plot of NMDS was generated by CANOCO 5 software (Microcomputer Power, Ithacha, NY, USA).

3. Results and Discussion

3.1. Water Chemistry Properties

The in situ water chemistry parameters of the three sampling sites were presented in Table 2. In SW, there was no significant difference in their hydrochemical properties. The water temperature was close to 25 °C, and the water was in weakly alkaline and oxic condition. Since the water depths in OR (16.1 m) and NB (10.4 m) were higher than that in NS (7.0 m), the water temperature and dissolved oxygen (DO) concentration of OW in OR and NB were lower than those in NS. In OW, pH indicated a weak acid condition in NB with respect to weak alkaline condition in OR and NS. Moreover, OR and NB were under suboxic conditions, while NS was under oxic condition [1]. That is, from the original reservoir subregion to newly submerged bottom and slope subregions, the dissolved oxygen (DO) level in OW gradually increased as the water temperature increased and the water depth decreased.

Table 2. In situ information of the sampling sites in LLJ.

Sampling Site	Water Layer	Water Depth(m)	pH Values	Water Temperature (°C)	DO (mg/L)	Sediment Area (m^2)
OR	SW	0.5	8.07	25.2	4.40	-
	OW	16.1	7.15	21.6	1.14	31,836
NB	SW	0.5	8.07	25.1	4.29	-
	OW	10.4	6.60	24.3	2.71	138,427
NS	SW	0.5	8.07	25.0	4.14	-
	OW	7.0	8.02	24.6	4.09	213,168

3.2. Spatial Distributions of DOC and Optical Indicators

3.2.1. DOC Concentrations and Benthic Flux

The DOC concentrations of SW, OW, and PW were shown in Figure 2. On all sampling sites, the average DOC concentrations were higher in PWs (53.7 ± 16.6 mg/L) than in OWs (23.1 ± 1.4 mg/L) and SWs (22.7 ± 0.5 mg/L). This reveals that it might exist a potential upward release of DOC across the sediment-water interface in LLJ. Among these sampling sites, there was little difference in DOC concentration for overlying water, whereas significant difference existed between OR and NB ($p < 0.01$) as well as OR and NS ($p < 0.05$) for PW. Concretely, the average DOC concentration of PW in OR (66.9 ± 17.0 mg/L) was higher than those in NB (44.6 ± 4.7 mg/L) and NS (46.7 ± 15.8 mg/L). This is probably because the sediments stemming from original reservoir had longer sedimentary history, thicker peat layer, and more abundant organic matters than newly submerged regions [21,24]. Moreover, the terrain of original reservoir and newly submerged bottom regions is relatively flat, and the flatness is conducive to the accumulation of particles and organic debris. Faster sedimentation means that more fresh organic materials could be preserved in original reservoir subregion, other than consumed by respiration [41]. Moreover, the energy generated by anaerobic pathways is lower than that by aerobic respiration, and its supply of alternative electron receptors is often limited, which made the degradation efficiency of organic matter lower and thus leaded to further accumulation of organic matters in surface sediment of OR and NB [42].

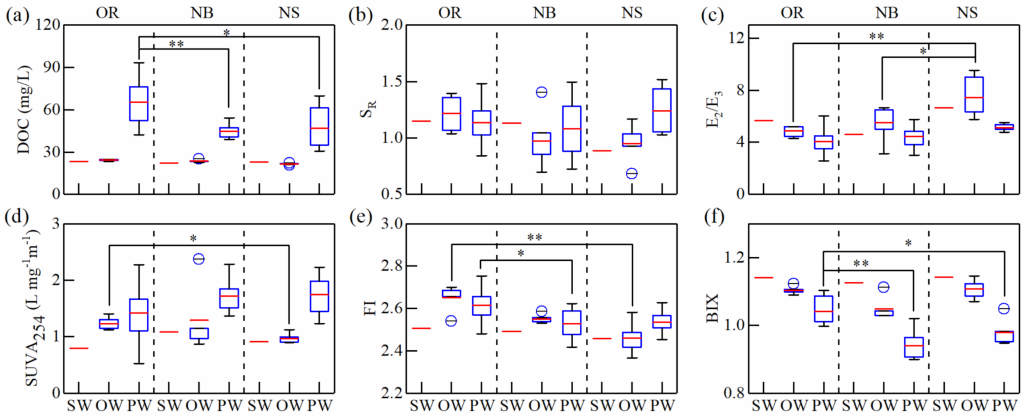

Figure 2. Box plots of (**a**) DOC concentrations; (**b**) S_R: spectral slope ratio; (**c**) E_2/E_3: absorption ratio; (**d**) $SUVA_{254}$: specific UV absorbance at 254 nm; (**e**) FI: Fluorescence index; (**f**) BIX: biological index) in SW, OW and PW from three sampling sites (OR, NB and NS). The symbols * and ** show significant differences at $p < 0.05$ and $p < 0.01$, respectively.

To further explore the contribution of DOC in sediment PW to OW, Fick's first law was used to estimate the benthic diffusion fluxes. The estimated DOC fluxes in the original reservoir region (OR, 88.3 mg m^{-2} d^{-1}) is higher than that in the newly submerged region (26 mg m^{-2} d^{-1}). More precisely, DOC fluxes in OR, NB, and NS were 88.3, 39.9, and

12.1 mg m^{-2} d^{-1}, respectively. The positive values validated that the LLJ sediments act as DOC sources to the overlying water. This benthic efflux is principally attributed to the degradation of sediment organic matter [43] and the reduction of redox-sensitive materials [44]. The DOC flux in OR herein is 2.2 and 7.3 times to those in NB and NS, and it is slightly higher than that of the hypoxic simulation result abstained by Yang, Choi and Hur [9]. This high flux was closely related with high DOC concentration in OR surface sediment. Subsequently taking the bottom sediment area into consideration, the estimated DOC annual load in LLJ was 3.99 t/a; and the DOC annual loads in OR, NB, and NS were 1.03, 2.02, and 0.94 t/a, respectively. Although the benthic efflux of DOC from original reservoir subregion was relatively large, the DOC annual load from newly submerged subregion accounted for 74% of the whole lake, serving as the main contribution region of DOC release. T

3.2.2. Spatial Distributions of Optical Indicators

Five optical indicators (S_R, E_2/E_3, $SUVA_{254}$, FI, and BIX) mentioned in Table 1 were used to reveal the sources and features of DOM. The first two indicators (S_R and E_2/E_3) are related to the apparent molecular weight of chromophoric DOM (CDOM) [30]. S_R represents the ratio of low-molecular-weight (LMW) to high-molecular-weight (HMW) CDOM [45], whereas E_2/E_3 stands for the relative molecular size of CDOM molecules [29]. The averages of S_R (> 1) in SW of OR and NB show that their LMW fractions of CDOM are higher than corresponding HMW fractions. This reveals that algal biomass, macrophyte, and microorganisms might make significant contribution to DOM in SW of the open areas [46]. Moreover, photo-bleaching could destroy chromophores associated with HMW CDOM and simultaneously increases its LMW fraction in OR and NB [16,28]. On the contrary, NS is located close to the lakeshore and is affected by terrestrial plant detritus or soil leachates from the surrounding watersheds, with S_R < 1 in SW and OW [47]. The second indicator (E_2/E_3) decreases as molecular size increases since HMW CDOM have strong capability of absorbing light at long wavelengths [28]. The averages of E_2/E_3 in OWs of three sampling sites were all higher than those in PWs reflecting that PWs have bigger molecular size of CDOM molecules.

The third indicator ($SUVA_{254}$), as an established proxy for aromaticity [32], is usually used to reflect the source and diagenetic status of sediment DOM [9,16,18]. $SUVA_{254}$ values tends to gradually increase from SW to PW, which refers to the preferential removal of aliphatic compounds during sedimentation [48]. The intrinsic photosensitivity of aromatic compounds also leads to their preferential degradation when sunlight penetrates the SW [49]. Previous studies revealed that refractory aromatic compounds tend to be preferentially preserved in sediments where exists liable organic substances releasing from sediment to overlying water [5]. In addition, the highest $SUVA_{254}$ values in PW are consistent with previous studies in inland and costal sediments where sediment DOM involved in highly aromatic compounds and is rich in N- and S-containing compounds [5,16,19]. Moreover, the order of averages of $SUVA_{254}$ in PWs is OR (1.42) < NB (1.72) < NS (1.74). Combined with the sedimentary background, it is speculated that the proportion of autochthonous DOM in the sediments of the original reservoir region is relatively high.

The last two indicators (FI and BIX) validate that the DOM in LLJ is of strong autochthonous characteristics. FI is commonly used to distinguish precursor organic materials for DOM, differentiating whether they are of more microbial (FI ~1.9) in nature or more terrestrially derived (FI ~1.4) [34]. The FI values among all water samples ranged from 2.42 to 2.75 (FI > 1.9), manifesting the predominance of microbial precursor materials for DOM [34]. These materials mainly stem from extracellular release as well as leachate from bacteria or algae [50]. The averages of FI in PWs follow the order of OR (2.62) > NS (2.54) > NB (2.53), demonstrating that the proportion of autochthonous DOM in the sediments of the original reservoir is higher than newly submerged region.

BIX is capable of indicating the proportion of DOM recently produced [35]. The BIX values in SW and OW were greater than 1.0, suggesting fresh DOM in LLJ predominantly

originates from autochthonous sources, i.e. biological or aquatic bacterial origin [35]. The greatest BIX values existed in SW. This probably because the growth of microbes and phytoplankton are stimulated by the bioavailable LMW organic compounds and inorganic nutrients, both of which could be produced by the photolysis of DOM in SW [51]. In accordance with $SUVA_{254}$, the proportion of recent autochthonous DOM in the sediments of the original reservoir region is higher than the newly submerged regions. Excepted the sedimentary background, this is probably related to the inefficient organic mineralization caused by anaerobic respiration of microorganisms, which causes the accumulation of newly formed DOM [42].

3.3. Composition of Fluorescent PARAFAC Components

According to PARAFAC analysis and Coble [52]'s classification, four components were identified (Figure 3 and Table 3): two humic-like (C1 and C3), one protein-like (C2), and one linked to autochthonous production (C4). Both components 1 and 3 are assigned to terrestrial humic-like fluorophores, despite the discrepancies in emission and excitation locations. C1, with the Ex/Em wavelengths of <225/415 nm, is similar to peak A [52] and belongs to HMW and aromatic humus [50]. It exists widespread in both terrestrial and marine environments [52] and usually serves as the predominant fluorophore [39]. C3 had an emission maximum at 445 nm and an excitation maximum at 260 nm and a shoulder at 360 nm. This component has similar fluorescence spectra with peak C [52]. Peaks A and C are primarily derived from vascular plants which have highly aromatic and conjugated structures, probably representing the HMW constituent of the DOM pool [50,53]. Although fluorophores A and C have similar source, the latter appears to be decomposed independently faster than the former [52].

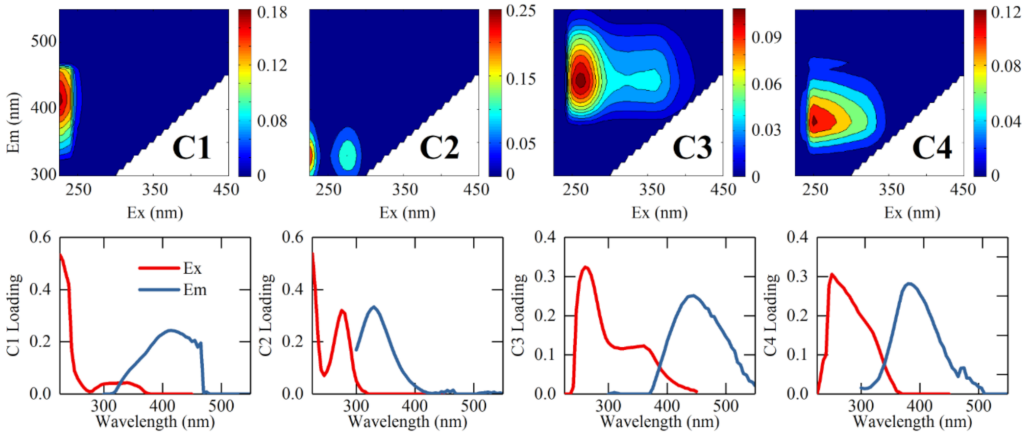

Figure 3. Contour plots of the four components identified by PARAFAC analysis (lower panel) and the locations of Emission (Ex) and Excitation (Ex) spectra of each component (upper panel).

Component 2, with the Ex/Em wavelengths of <250(275)/330 nm, resembles tryptophan-like fluorophore (peak T) [53]. Tryptophan, exhibiting peak T in natural water, presents as free molecules or bound in proteins, peptides or humic structures [54]. It is notable that lignin and simple phenols also emit similar fluorescence (Ex = 280 nm, Em = 325 nm) [55–57] and appear to contribute to the F_{max} of C2. This component is mainly derived from terrestrial plant, soil organic matter (allochthonous), autochthonous production, or microbial processing (autochthonous) [50]. It usually acts as an indicator of bioavailable, labile organic substrate or the product of microbial or algal activities [58,59]. "T1" and "T2" denote the left and right fluorescence peaks, respectively [60]. The F_{max} at peak T1 is higher than that at peak T2, which is consistent with that of peak T_{UV} and T in sediment PW of Yangtze River estuary [14,15], Lake Bosten, Lake Chenghai, and Lake Dianchi [19].

Component 4, with the Ex/Em wavelengths of 255(295)/385 nm, was assigned to microbial humic-like component [18] and described as peak M [52]. Despite peak M was

originally ubiquitous in marine waters linked with biological activity [52], it was also observed existing in wastewater, wetland, and agricultural environments [50]. Moreover, peak M has a "blue-shifted" emission peak (i.e., shift to shorter wavelength) compared to peaks A and C and is regarded as less aromatic, lower MW and richer aliphatic structures [52,60]. The possible sources of this component are the same as those of C2 [50].

Table 3. Comparing the four components at different Ex/Em peak locations from different classifications with those in existing literature.

Ex_{max}/Em_{max} (nm/nm)	Traditional Classification [52]	Comp.	Previous Findings								Assignment [13,18]
			I	II	III	IV	V	VI	VII	VIII	
<225/415	A	C1	C2	C2	C1	C1	C2	C3	C1	C1	Terrestrial humic-like
<225(275)/330	T	C2	C5	C4	C3	C2	C3	C2	C3	C3	Protein-like
260(360)/445	C	C3	C4	C3	C2	C3	C1	C4	C2	C2	Terrestrial humic-like
255(295)/385	M	C4	-	C1	–	–	–	–	–	–	Microbial humic-like

References: I [13]; II [18]; III [14]; IV [15]; V [61]; VI [16]; VII [20]; VIII [17].

3.4. Spatial Distribution of Fluorescent PARAFAC Components

The F_{max} and percentage of four fluorescent components were shown in Figure 4. The humic-like components (C1, C3 and C4) approximately accounted for 74% of total F_{max} in SW, 66% in OW, and 62% in PW, respectively; in correspondence, the protein-like component (C2) separately accounted for 26%, 32% and 38%.in SW, OW, and PW. The proportions of four FDOM components together with the indicators of FI and BIX indicate that FDOM is contributed by mixed sources in LLJ, comprising allochthonous and autochthonous sources. The former source acts as the predominant contributor and the latter also contributes an unneglectable proportion.

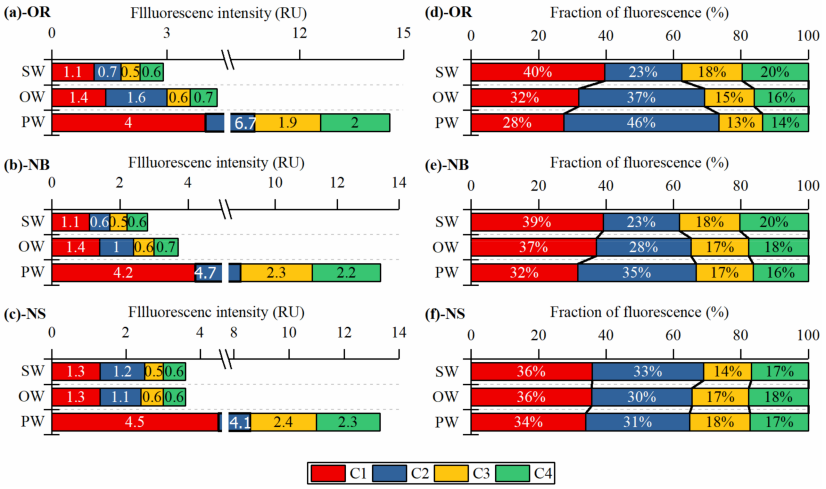

Figure 4. Bar charts of the F_{max} of four components in SW, OW and PW from (**a**) OR, (**b**) NB, (**c**) NS; and the percentage of each component to total F_{max} in SW, OW and PW from (**d**) OR, (**e**) NB, (**f**) NS.

The total F_{max} of PWs in OR (14.6 RU), NB (13.3 RU) and NS (13.2 RU) are 3.3, 3.6, and 3.8 times those of their corresponding OWs, respectively. This implies that labile FDOM has the potential to release from PW to OW [62], consistent with the above results of DOC concentrations. In contrast, the low F_{max} of SW in LLJ might be related to the long water residence time which increases the attenuation of DOM [63].

The F_{max} of C1 and C3 have no apparent difference in surface and overlying waters; at the same time, the F_{max} of C1 is greater than that of C3. This relationship probably correlates

with the molecular structure and origin of these components. C1 is considered to be a photo-resistant component stable in water environment [64] and partially preserved in sediments at last, while C3 is associated with both N-free vascular plant-derived compounds and is more aliphatic, oxygen-depleted molecules [6]. Since C3 is susceptible to be degraded when the water residence time is long [6], its content is low in SWs and OWs. Some investigations also found that the reduction of florescence similar to peak C3 co-occurred with increment in florescence similar to peak C1 [65,66], suggesting C1 is a degradation product of C3 [6]. Thus, in SW some moieties of the aromatic, oxidized, terrestrial component (C3) with long excitation-emission peak could be destroyed and transformed into more reduced molecules (C1) [6,62].

The F_{max} of C2 and C4 in PW are greater than those in OW and SW. In PW, the percentages of C2 to the total F_{max} (C2%) are higher in OR (46%) than in NB (35%) and NS (31%). One possible explanation is that the sediment in original reservoir region has abundant organic matter, and the anaerobic environment is more conducive to the storage of authigenic DOM. This is consistent with the results revealed by the indicators of $SUVA_{254}$, FI and BIX. In addition, few recalcitrant DOM produced in situ with elemental ratios similar to lignin might be mistaken as C2, which actually are carboxylic-rich alicyclic molecules [6,67].

3.5. Potential Influential Factors to DOM Distribution Behavior

NMDS analysis was employed to elucidate the dissimilarities of water samples based on their spectral properties, and the corresponding results are presented as an ordination diagram in Figure 5. The Euclidean distances between spots in ordination space correspond to dissimilarities: the larger the distance, the more obvious the dissimilarity [68]. Based on their similarity, the water samples are roughly divided into four groups as denoted by the dash oval circles. Group 1 comprises all SW and OW samples clustering at the negative end of NMDS 1; group 2 the top layers of PWs in OR (0–3 cm) and NB (0–1 cm); group 3 the PWs of deep layers in OR (5–10 cm) and middle layers in NB (2–6 cm) and in NS (2–4 cm); group 4 the PWs of deep layers in NB (6–10 cm) and middle layers in NS (4–6 cm).

Here the angle between two arrow lines of spectral indicators reveals the correlation between individual indicators [68]. The potential relationships were also quantified using spearman correlation, as demonstrated in Table 4. The terrestrial humic-like components (C1 and C3) were significantly associated with the in situ produced C4 (Spearman correlation: 0.98 and 0.97, $p < 0.01$), as suggested by the overlapping arrows in Figure 5 (C1, C3 and C4). The colorful symbols can be projected perpendicularly onto an arrow line (representing an individual indicator) of which the coordinate origin represents mean value. Projections at the direction towards the arrow denote values greater than the mean value, and vice versa those in the reverse direction are less than mean value [68]. The ordination graph illustrates that the symbols in groups 3 and 4 are generally close to the positive directions of C1, C3, and C4. Those in group 2 are close to the coordinate origin and those in group 1 close to their reverse directions. That is to say, the F_{max} of humic-like components in PWs suggest a gradual increase trend from the surface to deep sediments, and they are far greater than those of SWs and OWs.

Moreover, the humic-like components (C1, C3 and C4) were significant positive correlation with the adjacent $SUVA_{254}$ (Spearman correlation: 0.79, 0.78 and 0.78, respectively, $p < 0.01$), and negative correlation with BIX (Spearman correlation: -0.82, -0.85 and -0.82, respectively, $p < 0.01$). This suggests that the higher the content of humic-like components in DOM, the stronger its aromaticity. The contents of humus-like components of DOM in PWs are relatively high in deep sediments of both original reservoir and newly submerged regions. Group 1 together with the above-mentioned five indicators manifests that OWs and SWs are of high microbial activity, large amount of fresh DOM, and weak aromaticity and humification.

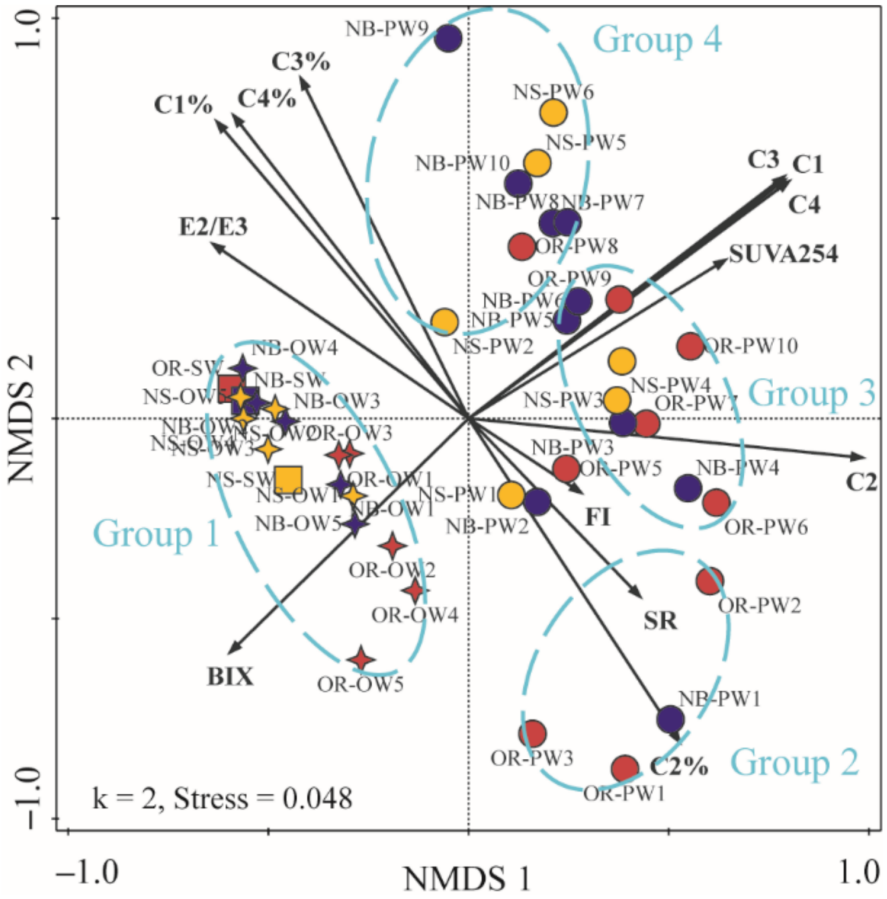

Figure 5. NMDS analysis of all spectral indicators for 44 water samples from three sampling sites. The ordination is generated based on Bray–Curtis distance (k = 2, stress = 0.048). The Squre, circle and star symbols separately represent SW, OW and PW samples. The colours red, blue and orange represent the sampling sites of OR, NB and NS, respectively. The Black arrow lines represent the spectral indicators, such as E_2/E_3, S_R, FI, BIX.

Table 4. Spearman correlations among DOC concentration, spectral indicators, and FDOM components.

	S_R	$SUVA_{254}$	E_2/E_3	FI	BIX	C1	C2	C3	C4	C1%	C2%	C3%	C4%	DOC
S_R	1		**				**			**	**	**	**	*
$SUVA_{254}$	-	1	*		**	**	**	**	**					**
E_2/E_3	−0.631	−0.369	1	*		*	**		*	**	**	**	**	**
FI	-	-	−0.311	1										
BIX	-	−0.682	-	-	1	**	**	**	**					**
C1	-	0.793	−0.301	-	−0.816	1	**	**	**					**
C2	0.435	0.616	−0.679	-	−0.545	0.716	1	**	**	**	**	**	**	**
C3	-	0.78	-	-	−0.852	0.982	0.692	1	**					**
C4	-	0.784	−0.303	-	−0.819	0.981	0.737	0.97	1					**
C1%	−0.53	-	0.671	-	-	-	−0.727	-	-	1	**	**	**	**
C2%	0.555	-	−0.671	-	-	-	0.679	-	-	−0.97	1	**	**	**
C3%	−0.445	-	0.551	-	-	-	−0.538	-	-	0.854	−0.931	1	**	*
C4%	−0.615	-	0.697	-	-	-	−0.664	-	-	0.903	−0.949	0.854	1	**
DOC	0.307	0.502	−0.65	-	−0.574	0.75	0.861	0.737	0.745	−0.507	0.443	−0.338	−0.47	1

** Correlation is significant at the 0.01 level (2-tailed); * Correlation is significant at the 0.05 level (2-tailed).

C2% was significant negative association with C1%, C3%, and C4% (Spearman correlation: −0.97, −0.93 and −0.95, respectively, $p < 0.01$). It should be noted that the symbols in group 2 are close to the positive direction of C2%. This manifests the highest proportions of protein-like component exist in PWs of both OR (0–3 cm) and NB (0–1 cm). The

affinity among group 2, C2%, FI and S_R suggests that the FDOM in surface sediments of OR and NB mainly attributes to the autochthonous productions, and there accumulates abundant fresh DOM. This is primarily related to their differently depositional history and environmental condition of the sampling sites. Neither the OR nor NB had been dredged before the impoundment of LLJ as mentioned above in Section 2. OR sediment is in strong reducing status and has abundant organic substances, which facilitates the respiration and metabolism of anaerobic microorganisms. Moreover, NB used to be mountain forest or farmland and still remains the original vegetation and soils after impoundment. These remnants caused the high OM and microbial activity in surface sediments of NB. In contrast, the bottom region of NS was mainly bare soil and gravel before impoundment. The low concentration of DOM in its surface sediments probably result in the relatively strong material decomposing and transforming driven by microorganisms [18]. Additionally, combined with the vertical change trend of these components, C2 was important fluorescent component in NB and NS water samples and sensitive to redox conditions along the vertical profile of OR sediments [7]. Thus, the F_{max} of C2 is a useful indicator in terms of revealing the changes of source of FDOM.

4. Conclusions

The optical properties of DOM in SWs, OWs and PWs of a nascent river-type lake were explored through five optical indicators and four fluorescence components. The conclusions are drawn as follows.

(1) In LLJ, the average DOC concentrations are higher in PWs than both in OWs and SWs, and the sediment acts as a DOC source to the OW. It is estimated that the DOC fluxes in original reservoir were higher than that in newly submerged region, while newly submerged region contributes the main portion of DOC release, accounting for 74% of the DOC annual load.

(2) In SW of the open region, the LMW fraction of CDOM is higher than the corresponding HMW fraction. Sediment PWs have higher aromaticity and lower proportion of fresh DOM than those in overlying waters. The surface sediments have relatively active microbial activity and low aromaticity compared with deep layers.

(3) Four fluorescent components were identified: C1 and C3 are terrestrial humic-like components, C2 protein-like, and C4 microbial humic-like. FDOM in this lake is contributed by mixed sources comprising both allochthonous and autochthonous sources. In surface sediments of original reservoir and newly formed bottom subregions, FDOM is mainly contributed by autochthonous source, others are mainly contributed by allochthonous source. Due to the high sensitivity of C2, it is a useful indicator to reveal the changes of source of FDOM.

Author Contributions: Conceptualization, F.N. and F.J.; methodology, F.N. and Q.S.; validation, formal analysis, investigation, visualization, data curation, writing—original draft preparation, F.N.; resources, F.J.; writing—review and editing, F.N., F.J., Q.Z., Q.S.; supervision, project administration, funding acquisition, F.J. All authors have read and agreed to the published version of the manuscript.

Funding: This research was funded by NATIONAL KEY R&D PROGRAM OF CHINA, grant number 2018YFD1100501; and funded by CHINA THREE GORGES COORPORATION ENVIRONMENT PROTECTION PROJECT, grant number 0799562.

Institutional Review Board Statement: Not applicable.

Informed Consent Statement: Not applicable.

Data Availability Statement: The data presented in this study are available in [Contrasting the Optical Characterization of Dissolved Organic Matter in Water and Sediment from a Nascent River-Type Lake (Chongqing, China)].

Acknowledgments: We wish to thank Chen Shijun for his language proofing for this manuscript.

Conflicts of Interest: The authors declare no conflict of interest.

References

1. Chen, M.L.; Kim, S.H.; Jung, H.J.; Hyun, J.H.; Choi, J.H.; Lee, H.J.; Huh, I.A.; Hur, J. Dynamics of dissolved organic matter in riverine sediments affected by weir impoundments: Production, benthic flux, and environmental implications. *Water Res.* **2017**, *121*, 150–161. [CrossRef] [PubMed]
2. Zuijdgeest, A.; Wehrli, B. Carbon and nutrient fluxes from floodplains and reservoirs in the Zambezi basin. *Chem. Geol.* **2017**, *467*, 1–11. [CrossRef]
3. Maavara, T.; Lauerwald, R.; Regnier, P.; Van Cappellen, P. Global perturbation of organic carbon cycling by river damming. *Nat. Commun.* **2017**, *8*, 15347. [CrossRef] [PubMed]
4. Wang, K.; Pang, Y.; He, C.; Li, P.; Xiao, S.; Sun, Y.; Pan, Q.; Zhang, Y.; Shi, Q.; He, D. Optical and molecular signatures of dissolved organic matter in Xiangxi Bay and mainstream of Three Gorges Reservoir, China: Spatial variations and environmental implications. *Sci. Total Environ.* **2019**, *657*, 1274–1284. [CrossRef] [PubMed]
5. Chen, M.; Hur, J. Pre-treatments, characteristics, and biogeochemical dynamics of dissolved organic matter in sediments: A review. *Water Res.* **2015**, *79*, 10–25. [CrossRef] [PubMed]
6. Kellerman, A.M.; Kothawala, D.N.; Dittmar, T.; Tranvik, L.J. Persistence of dissolved organic matter in lakes related to its molecular characteristics. *Nat. Geosci.* **2015**, *8*, 454–457. [CrossRef]
7. Meingast, K.M.; Grunert, B.K.; Green, S.A.; Kane, E.S.; Khademimoshgenani, N. Insights on Dissolved Organic Matter Production Revealed by Removal of Charge-Transfer Interactions in Senescent Leaf Leachates. *Water* **2020**, *12*, 2356. [CrossRef]
8. Freixa, A.; Ejarque, E.; Crognale, S.; Amalfitano, S.; Fazi, S.; Butturini, A.; Romani, A.M. Sediment microbial communities rely on different dissolved organic matter sources along a Mediterranean river continuum. *Limnol. Oceanogr.* **2016**, *61*, 1389–1405. [CrossRef]
9. Yang, L.; Choi, J.H.; Hur, J. Benthic flux of dissolved organic matter from lake sediment at different redox conditions and the possible effects of biogeochemical processes. *Water Res.* **2014**, *61*, 97–107. [CrossRef]
10. Withers, P.J.A.; Jarvie, H.P. Delivery and cycling of phosphorus in rivers: A review. *Sci. Total Environ.* **2008**, *400*, 379–395. [CrossRef]
11. Schmidt, F.; Koch, B.P.; Goldhammer, T.; Elvert, M.; Witt, M.; Lin, Y.-S.; Wendt, J.; Zabel, M.; Heuer, V.B.; Hinrichs, K.-U. Unraveling signatures of biogeochemical processes and the depositional setting in the molecular composition of pore water DOM across different marine environments. *Geochim. Cosmochim. Acta* **2017**, *207*, 57–80. [CrossRef]
12. Burdige, D.J.; Kline, S.W.; Chen, W.H. Fluorescent dissolved organic matter in marine sediment pore waters. *Mar. Chem.* **2004**, *89*, 289–311. [CrossRef]
13. Osburn, C.L.; Handsel, L.T.; Mikan, M.P.; Paerl, H.W.; Montgomery, M.T. Fluorescence Tracking of Dissolved and Particulate Organic Matter Quality in a River-Dominated Estuary. *Environ. Sci. Technol.* **2012**, *46*, 8628–8636. [CrossRef] [PubMed]
14. Wang, Y.; Zhang, D.; Shen, Z.Y.; Feng, C.H.; Chen, J. Revealing Sources and Distribution Changes of Dissolved Organic Matter (DOM) in Pore Water of Sediment from the Yangtze Estuary. *PLoS ONE* **2013**, *8*, e76633. [CrossRef] [PubMed]
15. Wang, Y.; Zhang, D.; Shen, Z.Y.; Chen, J.; Feng, C.H. Characterization and spacial distribution variability of chromophoric dissolved organic matter (CDOM) in the Yangtze Estuary. *Chemosphere* **2014**, *95*, 353–362. [CrossRef] [PubMed]
16. He, W.; Jung, H.; Lee, J.H.; Hur, J. Differences in spectroscopic characteristics between dissolved and particulate organic matters in sediments: Insight into distribution behavior of sediment organic matter. *Sci. Total Environ.* **2016**, *547*, 1–8. [CrossRef]
17. Lee, M.H.; Jung, H.J.; Kim, S.H.; An, S.U.; Choi, J.H.; Lee, H.J.; Huh, I.A.; Hur, J. Potential linkage between sediment oxygen demand and pore water chemistry in weir-impounded rivers. *Sci. Total Environ.* **2018**, *619–620*, 1608–1617. [CrossRef]
18. Ziegelgruber, K.L.; Zeng, T.; Arnold, W.A.; Chin, Y.P. Sources and composition of sediment pore-water dissolved organic matter in prairie pothole lakes. *Limnol. Oceanogr.* **2013**, *58*, 1136–1146. [CrossRef]
19. Mostofa, K.M.G.; Li, W.; Wu, F.C.; Liu, C.Q.; Liao, H.Q.; Zeng, L.; Xiao, M. Environmental characteristics and changes of sediment pore water dissolved organic matter in four Chinese lakes. *Environ. Sci. Pollut. Res.* **2018**, *25*, 2783–2804. [CrossRef]
20. Chen, Y.H.; Yu, K.F.; Zhou, Y.Q.; Ren, L.F.; Kirumba, G.; Zhang, B.; He, Y.L. Characterizing spatiotemporal variations of chromophoric dissolved organic matter in headwater catchment of a key drinking water source in China. *Environ. Sci. Pollut. Res.* **2017**, *24*, 27799–27812. [CrossRef]
21. Pan, Y.; Lei, P.; Zhang, H.; Shan, B.; Li, J. Distribution of nitrogen and phosphorus in the sediments and estimation of the nutrients fluxes in Longjinghu Lake, Chongqing City, during the initial impoundment period. *Environ. Sci.* **2014**, *35*, 1727–1734. (In Chinese)
22. Niu, F.; Ji, F.; Zhao, G.; Zhang, Q.; Shen, Q.; He, Q.; Yan, H. Vertical distribution of bacterial community structure in sediments of Longjing Lake, Chongqing, China. *China Environ. Sci.* **2017**, *37*, 2322–2331. (In Chinese)
23. Tian, T.; Zhang, D.; Li, Y.; He, Q.; Lu, P. Specific features of inorganic sulfur distribution and the effects of the organic contents in the Expo-Garden Longjing Lake, Chongqing. *J. Saf. Environ.* **2016**, *16*, 304–308. (In Chinese)
24. Ji, F.; Yan, H.; Zhao, G.; He, Q.; Niu, F. Distribution of nitrogen speciation at the sediment-water interface in Longjinggou Catchment Area of Longjinghu Lake. *China Environ. Sci.* **2015**, *35*, 3101–3107. (In Chinese)
25. Song, H.; Li, Z.; Du, B.; Wang, G.; Ding, Y. Bacterial communities in sediments of the shallow Lake Dongping in China. *J Appl Microbiol* **2012**, *112*, 79–89. [CrossRef] [PubMed]
26. Tan, E.; Zou, W.; Jiang, X.; Wan, X.; Hsu, T.-C.; Zheng, Z.; Chen, L.; Xu, M.; Dai, M.; Kao, S. Organic matter decomposition sustains sedimentary nitrogen loss in the Pearl River Estuary, China. *Sci. Total Environ.* **2019**, *648*, 508–517. [CrossRef] [PubMed]

27. Burdige, D.J.; Martens, C.S. Biogeochemical cycling in an organic-rich coastal marine basin: 11. The sedimentary cycling of dissolved, free amino acids. *Geochim. Cosmochim. Acta* **1990**, *54*, 3033–3052. [CrossRef]
28. Helms, J.R.; Stubbins, A.; Ritchie, J.D.; Minor, E.C.; Kieber, D.J.; Mopper, K. Absorption spectral slopes and slope ratios as indicators of molecular weight, source, and photobleaching of chromophoric dissolved organic matter. *Limnol. Oceanogr.* **2008**, *53*, 955–969. [CrossRef]
29. De Haan, H.; De Boer, T. Applicability of light absorbance and fluorescence as measures of concentration and molecular size of dissolved organic carbon in humic Lake Tjeukemeer. *Water Res.* **1987**, *21*, 731–734. [CrossRef]
30. Timko, S.A.; Gonsior, M.; Cooper, W.J. Influence of pH on fluorescent dissolved organic matter photo-degradation. *Water Res.* **2015**, *85*, 266–274. [CrossRef]
31. Zhou, Y.; Jeppesen, E.; Zhang, Y.; Shi, K.; Liu, X.; Zhu, G. Dissolved organic matter fluorescence at wavelength 275/342 nm as a key indicator for detection of point-source contamination in a large Chinese drinking water lake. *Chemosphere* **2016**, *144*, 503–509. [CrossRef] [PubMed]
32. Weishaar, J.L.; Aiken, G.R.; Bergamaschi, B.A.; Fram, M.S.; Fujii, R.; Mopper, K. Evaluation of specific ultraviolet absorbance as an indicator of the chemical composition and reactivity of dissolved organic carbon. *Environ. Sci. Technol.* **2003**, *37*, 4702–4708. [CrossRef] [PubMed]
33. Cory, R.M.; McKnight, D.M. Fluorescence spectroscopy reveals ubiquitous presence of oxidized and reduced quinones in dissolved organic matter. *Environ. Sci. Technol.* **2005**, *39*, 8142–8149. [CrossRef] [PubMed]
34. McKnight, D.M.; Boyer, E.W.; Westerhoff, P.K.; Doran, P.T.; Kulbe, T.; Andersen, D.T. Spectrofluorometric characterization of dissolved organic matter for indication of precursor organic material and aromaticity. *Limnol. Oceanogr.* **2001**, *46*, 38–48. [CrossRef]
35. Huguet, A.; Vacher, L.; Relexans, S.; Saubusse, S.; Froidefond, J.M.; Parlanti, E. Properties of fluorescent dissolved organic matter in the Gironde Estuary. *Org. Geochem.* **2009**, *40*, 706–719. [CrossRef]
36. Lawaetz, A.J.; Stedmon, C.A. Fluorescence Intensity Calibration Using the Raman Scatter Peak of Water. *Appl. Spectrosc.* **2009**, *63*, 936–940. [CrossRef]
37. Kothawala, D.N.; Murphy, K.R.; Stedmon, C.A.; Weyhenmeyer, G.A.; Tranvik, L.J. Inner filter correction of dissolved organic matter fluorescence. *Limnol. Oceanogr. Methods* **2013**, *11*, 616–630. [CrossRef]
38. Stedmon, C.A.; Bro, R. Characterizing dissolved organic matter fluorescence with parallel factor analysis: A tutorial. *Limnol. Oceanogr. Methods* **2008**, *6*, 572–579. [CrossRef]
39. Stedmon, C.A.; Markager, S.; Bro, R. Tracing dissolved organic matter in aquatic environments using a new approach to fluorescence spectroscopy. *Mar. Chem.* **2003**, *82*, 239–254. [CrossRef]
40. Zhou, Y.Q.; Zhang, Y.L.; Jeppesen, E.; Murphy, K.R.; Shi, K.; Liu, M.L.; Liu, X.H.; Zhu, G.W. Inflow rate-driven changes in the composition and dynamics of chromophoric dissolved organic matter in a large drinking water lake. *Water Res.* **2016**, *100*, 211–221. [CrossRef]
41. Chen, M.; Kim, J.H.; Nam, S.I.; Niessen, F.; Hong, W.L.; Kang, M.H.; Hur, J. Production of fluorescent dissolved organic matter in Arctic Ocean sediments. *Sci. Rep.* **2016**, *6*, 1–10. [CrossRef] [PubMed]
42. Burdige, D.J.; Komada, T.; Magen, C.; Chanton, J.P. Modeling studies of dissolved organic matter cycling in Santa Barbara Basin (CA, USA) sediments. *Geochim. Cosmochim. Acta* **2016**, *195*, 100–119. [CrossRef]
43. Burdige, D.J.; Komada, T. Sediment Pore Waters. In *Biogeochemistry of Marine Dissolved Organic Matter*, 2nd ed.; Hansell, D.A., Carlson, C.A., Eds.; Academic Press: Boston, MA, USA, 2015; pp. 535–577. [CrossRef]
44. Skoog, A.C.; Arias-Esquivel, V.A. The effect of induced anoxia and reoxygenation on benthic fluxes of organic carbon, phosphate, iron, and manganese. *Sci. Total Environ.* **2009**, *407*, 6085–6092. [CrossRef] [PubMed]
45. Twardowski, M.S.; Boss, E.; Sullivan, J.M.; Donaghay, P.L. Modeling the spectral shape of absorption by chromophoric dissolved organic matter. *Mar. Chem.* **2004**, *89*, 69–88. [CrossRef]
46. Bai, L.; Zhang, Q.; Wang, C.; Yao, X.; Zhang, H.; Jiang, H. Effects of natural dissolved organic matter on the complexation and biodegradation of 17α-ethinylestradiol in freshwater lakes. *Environ. Pollut.* **2019**, *246*, 782–789. [CrossRef]
47. Hansen, A.M.; Kraus, T.E.C.; Pellerin, B.A.; Fleck, J.A.; Downing, B.D.; Bergamaschi, B.A. Optical properties of dissolved organic matter (DOM): Effects of biological and photolytic degradation. *Limnol. Oceanogr.* **2016**, *61*, 1015–1032. [CrossRef]
48. Abdelrady, A.; Sharma, S.; Sefelnasr, A.; Kennedy, M. The Fate of Dissolved Organic Matter (DOM) During Bank Filtration under Different Environmental Conditions: Batch and Column Studies. *Water* **2018**, *10*, 1730. [CrossRef]
49. Stubbins, A.; Spencer, R.G.M.; Chen, H.M.; Hatcher, P.G.; Mopper, K.; Hernes, P.J.; Mwamba, V.L.; Mangangu, A.M.; Wabakanghanzi, J.N.; Six, J. Illuminated darkness: Molecular signatures of Congo River dissolved organic matter and its photochemical alteration as revealed by ultrahigh precision mass spectrometry. *Limnol. Oceanogr.* **2010**, *55*, 1467–1477. [CrossRef]
50. Fellman, J.B.; Hood, E.; Spencer, R.G.M. Fluorescence spectroscopy opens new windows into dissolved organic matter dynamics in freshwater ecosystems: A review. *Limnol. Oceanogr.* **2010**, *55*, 2452–2462. [CrossRef]
51. Lipczynska-Kochany, E. Humic substances, their microbial interactions and effects on biological transformations of organic pollutants in water and soil: A review. *Chemosphere* **2018**, *202*, 420–437. [CrossRef]
52. Coble, P.G. Characterization of marine and terrestrial DOM in seawater using excitation emission matrix spectroscopy. *Mar. Chem.* **1996**, *51*, 325–346. [CrossRef]

53. Coble, P.G.; Del Castillo, C.E.; Avril, B. Distribution and optical properties of CDOM in the Arabian Sea during the 1995 Southwest Monsoon. *Deep Sea Res. Part Ii Top. Stud. Oceanogr.* **1998**, *45*, 2195–2223. [CrossRef]
54. Hudson, N.; Baker, A.; Ward, D.; Reynolds, D.M.; Brunsdon, C.; Carliell-Marquet, C.; Browning, S. Can fluorescence spectrometry be used as a surrogate for the Biochemical Oxygen Demand (BOD) test in water quality assessment? An example from South West England. *Sci. Total Environ.* **2008**, *391*, 149–158. [CrossRef] [PubMed]
55. Coble, P.G. Marine optical biogeochemistry: The chemistry of ocean color. *Chem. Rev.* **2007**, *107*, 402–418. [CrossRef] [PubMed]
56. Maie, N.; Scully, N.M.; Pisani, O.; Jaffé, R. Composition of a protein-like fluorophore of dissolved organic matter in coastal wetland and estuarine ecosystems. *Water Res.* **2007**, *41*, 563–570. [CrossRef]
57. Hernes, P.J.; Bergamaschi, B.A.; Eckard, R.S.; Spencer, R.G.M. Fluorescence-based proxies for lignin in freshwater dissolved organic matter. *J. Geophys. Res. Biogeosci.* **2009**, *114*, G00F03. [CrossRef]
58. Cammack, W.K.L.; Kalff, J.; Prairie, Y.T.; Smith, E.M. Fluorescent dissolved organic matter in lakes: Relationships with heterotrophic metabolism. *Limnol. Oceanogr.* **2004**, *49*, 2034–2045. [CrossRef]
59. Elliott, S.; Lead, J.R.; Baker, A. Characterisation of the fluorescence from freshwater, planktonic bacteria. *Water Res.* **2006**, *40*, 2075–2083. [CrossRef]
60. Tedetti, M.; Cuet, P.; Guigue, C.; Goutx, M. Characterization of dissolved organic matter in a coral reef ecosystem subjected to anthropogenic pressures (La Reunion Island, Indian Ocean) using multi-dimensional fluorescence spectroscopy. *Sci. Total Environ.* **2011**, *409*, 2198–2210. [CrossRef]
61. Hur, J.; Lee, B.-M.; Shin, K.-H. Spectroscopic characterization of dissolved organic matter isolates from sediments and the association with phenanthrene binding affinity. *Chemosphere* **2014**, *111*, 450–457. [CrossRef]
62. Xiao, M.; Wu, F.; Yi, Y.; Han, Z.; Wang, Z. Optical Properties of Dissolved Organic Matter and Controlling Factors in Dianchi Lake Waters. *Water* **2019**, *11*, 1967. [CrossRef]
63. Kellerman, A.M.; Dittmar, T.; Kothawala, D.N.; Tranvik, L.J. Chemodiversity of dissolved organic matter in lakes driven by climate and hydrology. *Nat. Commun.* **2014**, *5*, 3804. [CrossRef] [PubMed]
64. Ishii, S.K.L.; Boyer, T.H. Behavior of Reoccurring PARAFAC Components in Fluorescent Dissolved Organic Matter in Natural and Engineered Systems: A Critical Review. *Environ. Sci. Technol.* **2012**, *46*, 2006–2017. [CrossRef] [PubMed]
65. Vecchio, R.D.; Blough, N.V. On the origin of the optical properties of humic substances. *Environ. Sci. Technol.* **2004**, *38*, 3885–3891. [CrossRef]
66. Kothawala, D.N.; von Wachenfeldt, E.; Koehler, B.; Tranvik, L.J. Selective loss and preservation of lake water dissolved organic matter fluorescence during long-term dark incubations. *Sci. Total Environ.* **2012**, *433*, 238–246. [CrossRef]
67. Hertkorn, N.; Benner, R.; Frommberger, M.; Schmitt-Kopplin, P.; Witt, M.; Kaiser, K.; Kettrup, A.; Hedges, J.I. Characterization of a major refractory component of marine dissolved organic matter. *Geochim. Cosmochim. Acta* **2006**, *70*, 2990–3010. [CrossRef]
68. Smilauer, P.; Lepš, J. *Multivariate Analysis of Ecological Data Using Canoco 5*; Cambridge University Press: New York, NY, USA, 2014; p. 193.